Journal of Fluids and Structures 18 (2003) 179–196

JOURNAL OF FLUIDS AND STRUCTURES

www.elsevier.nl/locate/jnlabr/yjfls

Exact solution of linear hyperbolic four-equation system in axial liquid-pipe vibration

A.S. Tijsseling*

Department of Mathematics and Computer Science, Eindhoven University of Technology, Den Dolech 2, P.O. Box 513, 5600 MB Eindhoven, The Netherlands

Received 12 May 2003; accepted 18 July 2003

Abstract

The so-called "FSI four-equation model" describes the axial vibration of liquid-filled pipes. Two equations for the liquid are coupled to two equations for the pipe, through terms proportional to the Poisson contraction ratio, and through mutual boundary conditions. In 1955 and 1956, Skalak defined this basic model, which disregards friction and damping effects.

The four equations can be solved with the method of characteristics (MOC). The standard approach is to cover the distance–time plane with equidistantly spaced grid-points and to time-march from a given initial state. This approach introduces error, because either numerical interpolations or wave speed adjustments are necessary.

This paper presents a method of exact calculation in terms of a simple recursion. The method is valid for transient events only, because the calculation time grows exponentially with the duration of the event. The calculation time is proportional to the temporal and spatial resolution. The exact solutions are used to investigate the error due to numerical interpolations and wave speed adjustments, with emphasis on the latter.

1. Introduction

1.1. FSI four-equation model

Classical waterhammer (fluid) and beam (structure) theories adequately describe the low-frequency vibration of liquid-filled pipe systems. The liquid is added mass in the lateral pipe vibration and it is neglected in the torsional pipe vibration. The role of the liquid in the axial pipe vibration has always been a point of discussion. Is it just (frequency-dependent) added mass (and stiffness)? Has its full elastic behaviour to be considered? And what fluid–structure interaction (FSI) mechanisms have to be taken into account? To answer these questions, the so-called "FSI four-equation model" has to be solved. The model describes the coupled axial vibration of liquid and pipe, where the coupling is through terms in the equations and through boundary conditions.

The four equations, governing fluid pressure, P, fluid velocity, V, axial pipe stress, σ_z, and axial pipe velocity, $\dot{u}_z$, are

$$\frac{\partial V}{\partial t}+\frac{1}{\rho_f}\frac{\partial P}{\partial z}=0, \tag{1}$$

$$\frac{\partial V}{\partial z}+\left(\frac{1}{K}+\frac{2R}{Ee}\right)\frac{\partial P}{\partial t}-\frac{2\nu}{E}\frac{\partial \sigma_z}{\partial t}=0, \tag{2}$$

*Tel.: +31-40-247-2755; fax: +31-40-244-2489.
E-mail address: a.s.tijsseling@tue.nl (A.S. Tijsseling).

0889-9746/$ - see front matter
doi:10.1016/j.jfluidstructs.2003.07.001

Nomenclature

Scalars

A	cross-sectional area (m^2)
c	classical wave speed (m/s)
c_d	damping coefficient (kg/s)
det	determinant
E	Young's modulus of pipe wall material (Pa)
e	pipe wall thickness (m)
FSI	fluid–structure interaction
K	fluid bulk modulus (Pa)
L	pipe length (m)
MOC	method of characteristics
P	fluid pressure (Pa)
R	inner radius of pipe (m)
T_c	valve closure time (s)
t	time (s)
$\dot{u}_z$	axial pipe velocity (m/s)
V	fluid velocity (m/s)
V_r	relative fluid velocity, $V - \dot{u}_z$ (m/s)
z	axial coordinate (m)
γ	constant (m/s), see Eq. (25)
Δ	numerical step size; change in magnitude
λ	eigenvalue, wave speed (m/s)
ν	Poisson ratio
ξ	loss coefficient
ρ	mass density (kg/m^3)
σ_z	axial pipe stress (Pa)
τ	valve closure function, see Eq. (34)

Matrices and vectors

$\mathbf{A}$	coefficients, see Eqs. (5) and (21)
$\mathbf{B}$	coefficients, see Eqs. (5) and (22)
$\mathbf{C}$	coefficients, see Eq. (5)
$\mathbf{D}$	boundary condition coefficients, see Eqs. (19) and (30)
$\mathbf{O}$	zero matrix
$\mathbf{q}$	excitation vector, see Eqs. (19)
$\mathbf{R}$	matrix, see Eq. (18)
$\mathbf{S}$	transformation matrix, see Eqs. (12) and (27)
$\mathbf{T}$	transformation matrix, see Eq. (27)
$\boldsymbol{\eta}$	Riemann invariants, see Eq. (6)
$\boldsymbol{\Lambda}$	diagonal matrix of eigenvalues, see Eq. (10)
$\boldsymbol{\xi}$	eigenvector, see Eq. (12)
$\boldsymbol{\phi}$	dependent variables, see Eqs. (5) and (20)

Subscripts

b	boundary
f	fluid, flow
L	boundary position $z = L$
r	relative
s	structure, solid
z	axial direction
0	boundary position $z = 0$; initial state $t = 0$

$$\frac{\partial \dot{u}_z}{\partial t} - \frac{1}{\rho_s}\frac{\partial \sigma_z}{\partial z} = 0, \tag{3}$$

$$\frac{\partial \dot{u}_z}{\partial z} - \frac{1}{E}\frac{\partial \sigma_z}{\partial t} + \frac{\nu R}{Ee}\frac{\partial P}{\partial t} = 0. \tag{4}$$

The model is valid for the low-frequency acoustic behaviour of straight, thin-walled, linearly elastic, liquid-filled, prismatic pipes of circular cross-section.

Skalak (1955/1956a, b) derived the FSI four-equation model as an extension of Joukowsky's method and as the low-frequency limit of two-dimensional fluid and shell representations. He showed that the model permits solutions that are waves of arbitrary shape travelling without dispersion at the phase velocity of either the liquid (λ_1) or the pipe (λ_3), but he made no attempt to solve the four equations in general. The validity of the FSI four-equation model has been demonstrated by many researchers, but most prominently by Vardy and Fan (1989). For more information on the subject the reader is referred to review papers by Tijsseling (1996), and Wiggert and Tijsseling (2001).

1.2. Conventional approach

The method of characteristics (MOC) is the preferred method to solve the FSI four-equation model, because the wave speeds are constant (no dispersion) and, unlike finite difference (Schwarz, 1978) and finite element (Zhang et al., 1994) methods, steep wave fronts can be properly dealt with. The distance–time plane is covered with either a rectangular (collocated) or a diamond (staggered) computational grid. To avoid interpolations and have Courant numbers equal to one, Schwarz (1978), Wiggert et al. (1985, 1987), Bürmann et al. (1987), Bürmann and Thielen (1988a, b) and others assumed wave speed ratios (λ_3/λ_1) that are whole numbers (integers). This strong assumption was relieved by Tijsseling (1993), Tijsseling et al. (1996), and Bergant and Tijsseling (2001) by allowing the wave speed ratios (λ_3/λ_1) to be rational numbers at the expense of refined computational grids. Fan (1989), Elansary and Contractor (1990), Bouabdallah and Massouh (1997) and others used interpolations on fine grids.

The conventional MOC approaches introduce phase error if wave speeds are adjusted, and numerical dispersion and damping if interpolations are employed. Both types of error accumulate when marching in time. Furthermore, for all approaches, interpolations are necessary when numerical data is required in between grid points, for example at the location of measuring devices.

1.3. New approach

The new approach presented in this paper has no interpolations, no adjustments (of wave speeds) and no approximations. It is valid for linear, non-dispersive, non-dissipative, hyperbolic systems with linear (or quadratic) time-dependent boundary conditions. It gives exact solutions without the errors of the conventional approaches.

The only previous exact solutions of the FSI four-equation model known to the author are due to Bürmann (1975), Williams (1977), and Wilkinson and Curtis (1980). Bürmann (1975) used the MOC to find all possible transmission and reflection coefficients in coaxial pipe systems. Williams (1977) applied jump conditions to calculate the initial effect of precursor waves (pressure changes caused by axial-stress waves) on waterhammer. Wilkinson and Curtis (1980), in an excellent paper, utilised jump conditions and reflection coefficients to calculate and explain the events in their laboratory experiment (Fig. 1). The applicability of jump conditions and reflection/transmission coefficients is limited, because all wave fronts have to be tracked to find exact solutions. Citing Williams (1977, p. 242): "each wave, be it precursor or waterhammer, in general gives rise to two reflected waves, one of each type: the resulting exponential growth in the number of separate waves in the pipe causes obvious analytical difficulties". Wilkinson and Curtis (1980, p. 240) simulated a time period of $5L/(2\lambda_1)$ in which 50 wave fronts existed. Tracking of these wave fronts and their strengths was done by hand (and not without error). Edwards and Please (1988) proposed a discrete analogue of the MOC, which was less laborious than the method of Wilkinson and Curtis, but they had to apply some averaging (interpolation) at the boundaries.

The present method automatically tracks wave fronts backward in time by means of a simple recursion. The exact solutions thus obtained can be used: to check numerical results and schemes, to confirm the accuracy of previous results, to serve as reference solutions in benchmark problems, and to perform parameter variation studies without parameter changes generated by the numerical method itself (e.g., changed wave speeds). The method does not require a conventional computational grid. It is general and can be applied to analogous four-equation systems encountered in, for example, the theory of linear(ized) waves in two-phase flows, two-layer density currents, and liquid-saturated

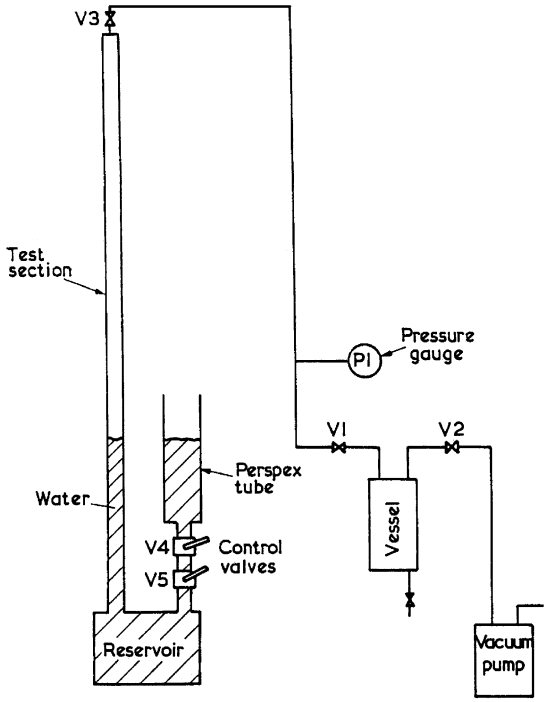

Fig. 1. Waterhammer rig of Wilkinson and Curtis (1980).

porous media. The method works also for higher-order systems like those developed by Bürmann (1975). In higher-order systems the necessary eigenvalues and eigenvectors cannot generally be found in closed form.

2. Theory

The analytical development follows (Zhang et al., 1999, Appendix A).

2.1. General equations

The general equations

$$\mathbf{A}\frac{\partial}{\partial t}\boldsymbol{\phi}(z,t)+\mathbf{B}\frac{\partial}{\partial z}\boldsymbol{\phi}(z,t)+\mathbf{C}\boldsymbol{\phi}(z,t)=\mathbf{0} \tag{5}$$

describe linear wave propagation in one spatial dimension. The constant matrices $\mathbf{A}$ and $\mathbf{B}$ are invertible and $\mathbf{A}^{-1}\mathbf{B}$ is diagonalizable. The constant matrix $\mathbf{C}$, which may be singular, causes frequency dispersion (if $\mathbf{C}\neq\mathbf{O}$). The N dependent and coupled variables ϕ_i, constituting the state vector $\boldsymbol{\phi}$, are functions of the independent variables z (space) and t (time). Herein $N=4$ and $\mathbf{C}=\mathbf{O}$.

2.2. Method of characteristics

The MOC introduces a new set of dependent variables through

$$\boldsymbol{\eta}(z,t)=\mathbf{S}^{-1}\boldsymbol{\phi}(z,t) \text{ or } \boldsymbol{\phi}(z,t)=\mathbf{S}\boldsymbol{\eta}(z,t), \tag{6}$$

so that each η_i is a linear combination of the original variables ϕ_i. Substitution of Eq. (6) into Eq. (5), with $\mathbf{C}=\mathbf{O}$, gives

$$\mathbf{AS}\frac{\partial}{\partial t}\eta(z,t)+\mathbf{BS}\frac{\partial}{\partial z}\boldsymbol{\eta}(z,t)=\mathbf{0}. \tag{7}$$

Multiplication by $\mathbf{S}^{-1}\mathbf{A}^{-1}$ yields

$$\frac{\partial}{\partial t}\boldsymbol{\eta}(z,t)+\boldsymbol{\Lambda}\frac{\partial}{\partial z}\boldsymbol{\eta}(z,t)=\mathbf{0}, \tag{8}$$

in which

$$\boldsymbol{\Lambda}=\mathbf{S}^{-1}\mathbf{A}^{-1}\mathbf{B}\mathbf{S}. \tag{9}$$

A set of decoupled equations is obtained when $\boldsymbol{\Lambda}$ is diagonal:

$$\boldsymbol{\Lambda}=\begin{pmatrix}\lambda_1 & 0 & 0 & 0\\ 0 & \lambda_2 & 0 & 0\\ 0 & 0 & \lambda_3 & 0\\ 0 & 0 & 0 & \lambda_4\end{pmatrix}. \tag{10}$$

Substitution of Eq. (10) into Eq. (9) and solving for $\mathbf{S}$ reveals that a non-trivial solution exists only when the diagonal elements of $\boldsymbol{\Lambda}$ are eigenvalues satisfying the characteristic equation

$$\det(\mathbf{B}-\lambda\mathbf{A})=0, \tag{11}$$

in which case $\mathbf{S}$ consists of the eigenvectors $\boldsymbol{\xi}_i$ of $\mathbf{A}^{-1}\mathbf{B}$ belonging to λ_i :

$$\mathbf{S}=\begin{pmatrix}\boldsymbol{\xi}_1 & \boldsymbol{\xi}_2 & \boldsymbol{\xi}_3 & \boldsymbol{\xi}_4\end{pmatrix}. \tag{12}$$

The decoupled Eq. (8),

$$\frac{\partial\eta_i(z,t)}{\partial t}+\lambda_i\frac{\partial\eta_i(z,t)}{\partial z}=0,\quad i=1,2,3,4 \tag{13}$$

transforms to

$$\frac{\mathrm{d}\eta_i(z,t)}{\mathrm{d}t}=0,\quad i=1,2,3,4 \tag{14}$$

when they are considered along characteristic lines in the $z-t$ plane defined by

$$\frac{\mathrm{d}z}{\mathrm{d}t}=\lambda_i,\quad i=1,2,3,4. \tag{15}$$

The solution of the ordinary differential Eqs. (14) and (15) is

$$\eta_i(z,t)=\eta_i(z-\lambda_i\Delta t,t-\Delta t),\quad i=1,2,3,4, \tag{16}$$

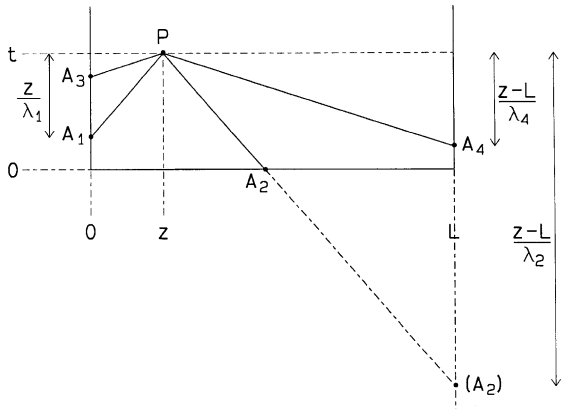

Fig. 2. Interior point P and "feeding" characteristic lines in the distance–time plane.

when a numerical time step Δt is used, or, more general and with reference to Fig. 2,

$$\eta_i(P) = \eta_i(A_i), \quad i = 1,2,3,4 \text{ or } \boldsymbol{\eta}(P) = \begin{pmatrix} \eta_1(A_1) \\ \eta_2(A_2) \\ \eta_3(A_3) \\ \eta_4(A_4) \end{pmatrix}. \tag{17}$$

The value of the unknown variable η_i does *not* change along the line A_iP.

The original unknowns in $\boldsymbol{\phi}$ are obtained from $\boldsymbol{\eta}$ through Eq. (6). This gives

$$\boldsymbol{\phi}(P) = \sum_{i=1}^{4} \mathbf{S}\mathbf{R}_i\mathbf{S}^{-1}\boldsymbol{\phi}(A_i), \tag{18}$$

where the ith diagonal element of the matrix $\mathbf{R}_i$ is 1 and all other elements are 0.

2.3. Boundary conditions

At the boundaries, the relations (16) or (17) provide two equations (see Fig. 3). To find the four unknowns $\eta_i(P)$ at the boundary $z = z_b$ ($z_b = 0$ or $z_b = L$), two additional equations are required. These are given by the linear boundary conditions

$$\mathbf{D}_{z_b}(t)\boldsymbol{\phi}(z_b,t) = \mathbf{q}_{z_b}(t) \quad \text{or} \quad \mathbf{D}_{z_b}(t)\mathbf{S}\boldsymbol{\eta}(z_b,t) = \mathbf{q}_{z_b}(t), \tag{19}$$

where $\mathbf{D}_{z_b}$ is a 2 by 4 matrix of coefficients and the 2-vector $\mathbf{q}_{z_b}$ is the (boundary) excitation. For convenience, the 4 by 4 matrix $\mathbf{D}$ combines the two matrices $\mathbf{D}_0$ and $\mathbf{D}_L$ by alternately stacking the rows of $\mathbf{D}_0$ and $\mathbf{D}_L$, and the 4-vector $\mathbf{q}$ combines the two vectors $\mathbf{q}_0$ and $\mathbf{q}_L$ by alternately stacking the rows of $\mathbf{q}_0$ and $\mathbf{q}_L$. Section 2.5 gives an example.

2.4. Initial conditions

The initial condition at $t = 0$ can be the steady state solution $\boldsymbol{\phi}(z,0) = \boldsymbol{\phi}_0$, where the constant state $\boldsymbol{\phi}_0$ is consistent with the boundary conditions, or it can be any non-equilibrium state $\boldsymbol{\phi}(z,0) = \boldsymbol{\phi}_0(z)$ exciting the system (e.g., sudden

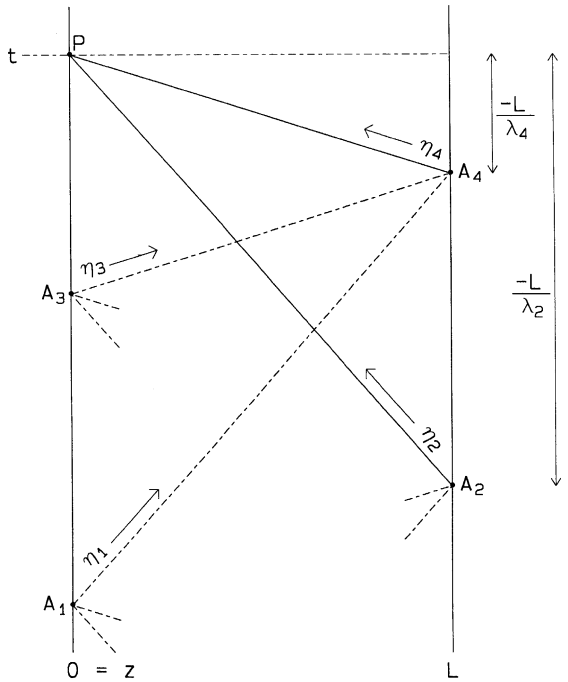

Fig. 3. Boundary point P and "feeding" characteristic lines in the distance–time plane.

release of pressure and/or stress). The once-only matrix inversion in $\boldsymbol{\eta}(z,0)=\mathbf{S}^{-1}\boldsymbol{\phi}_0(z)$ can be done algebraically (using Cramer's rule). Matrix inversion is not needed for zero initial conditions.

2.5. FSI four-equation model

In terms of the general Eq. (5), the axial vibration of a liquid-filled pipe (Eqs. (1)–(4)) can be represented by the state vector

$$\boldsymbol{\phi}=\begin{pmatrix} V \\ P \\ \dot{u}_z \\ \sigma_z \end{pmatrix} \tag{20}$$

and the matrices of coefficients

$$\mathbf{A}=\begin{pmatrix} 1 & 0 & 0 & 0 \\ 0 & (\rho_f c_f^2)^{-1} & 0 & 0 \\ 0 & 0 & 1 & 0 \\ 0 & \nu R(Ee)^{-1} & 0 & -(\rho_s c_s^2)^{-1} \end{pmatrix}, \tag{21}$$

$$\mathbf{B}=\begin{pmatrix} 0 & \rho_f^{-1} & 0 & 0 \\ 1 & 0 & -2\nu & 0 \\ 0 & 0 & 0 & -\rho_s^{-1} \\ 0 & 0 & 1 & 0 \end{pmatrix}. \tag{22}$$

The constants

$$c_f^2=\left[\frac{\rho_f}{K}+(1-\nu^2)\frac{2\rho_f R}{Ee}\right]^{-1} \text{ and } c_s^2=\frac{E}{\rho_s} \tag{23}$$

are the squares of the classical pressure and axial-stress wave speeds.

The characteristic (dispersion) Eq. (11), corresponding to the matrices (21) and (22), is

$$\lambda^4-\gamma^2\lambda^2+c_f^2c_s^2=0, \tag{24}$$

where

$$\gamma^2=\left(1+2\nu^2\frac{\rho_f}{\rho_s}\frac{R}{e}\right)c_f^2+c_s^2. \tag{25}$$

This leads to (slightly) modified (because of FSI) squared wave speeds

$$\lambda_{1,2}^2=\frac{1}{2}[\gamma^2-(\gamma^4-4c_f^2c_s^2)^{1/2}], \tag{26a}$$

$$\lambda_{3,4}^2=\frac{1}{2}[\gamma^2+(\gamma^4-4c_f^2c_s^2)^{1/2}], \tag{26b}$$

where λ_1 and λ_3 are positive, and λ_2 and λ_4 are negative.

The transformation matrix used (Eq. (12)) is $\mathbf{S}=(\mathbf{TA})^{-1}$ with $\mathbf{T}$ defined by

$$\begin{aligned} \text{row}_i\{\mathbf{T}\} &= \left(1,\lambda_i,2\nu\frac{\lambda_i^2}{c_s^2-\lambda_i^2},\ 2\nu\frac{c_s^2\lambda_i}{c_s^2-\lambda_i^2}\right) \quad i=1,2, \\ \text{row}_i\{\mathbf{T}\} &= \left(\rho_f\frac{\nu}{E}\frac{R}{e}\frac{c_f^2\lambda_i^2}{c_f^2-\lambda_i^2},\ \rho_f\frac{\nu}{E}\frac{R}{e}\frac{c_f^2\lambda_i^3}{c_f^2-\lambda_i^2},\ \frac{\lambda_i^2}{c_s^2},\lambda_i\right) \quad i=3,4. \end{aligned} \tag{27}$$

It is noted that transformation matrices are not unique. For example, $\mathbf{S}=(\mathbf{TB})^{-1}$ is an equally valid transformation matrix. The once-only matrix inversion of $\mathbf{TA}$ has been done numerically and, with the same result, algebraically (using Cramer's rule).

The boundary conditions are defined through coefficient matrices $\mathbf{D}$ and excitation vectors $\mathbf{q}$ (see Eq. (19)). For example, a reservoir at $z=0$ and an unrestrained massless valve at $z=L$, as in the Sections 4.1 and 4.2, give matrices

$$\mathbf{D}_0 = \begin{pmatrix} 0 & 1 & 0 & 0 \\ 0 & 0 & 1 & 0 \end{pmatrix} \quad \text{and} \quad \mathbf{q}_0 = \begin{pmatrix} 0 \\ 0 \end{pmatrix}, \tag{28}$$

$$\mathbf{D}_L = \begin{pmatrix} 1 & 0 & -1 & 0 \\ 0 & A_f & 0 & -A_s \end{pmatrix} \quad \text{and} \quad \mathbf{q}_L = \begin{pmatrix} 0 \\ 0 \end{pmatrix}, \tag{29}$$

where A is a cross-sectional area. In the author's previous work, e.g., Zhang et al. (1999), the above matrices and vectors have been simply stacked to form one matrix $\mathbf{D}$ and one vector $\mathbf{q}$. Herein, the boundary matrix $\mathbf{D}$ has rows with alternating the boundary conditions at $z = 0$ and $z = L$. Hence Eqs. (28) and (29) are combined to give

$$\mathbf{D} = \begin{pmatrix} 0 & 1 & 0 & 0 \\ 1 & 0 & -1 & 0 \\ 0 & 0 & 1 & 0 \\ 0 & A_f & 0 & -A_s \end{pmatrix} \quad \text{and} \quad \mathbf{q} = \begin{pmatrix} 0 \\ 0 \\ 0 \\ 0 \end{pmatrix}. \tag{30}$$

By taking $\mathbf{D}_{43} = -c_d$ the system is damped by a dashpot connected to the valve.

2.6. Nonlinear non-instantaneous valve closure

In steady turbulent pipe flow the pressure loss, ΔP_0, across a fully open valve is given by the orifice equation

$$\Delta P_0 = \xi_0 \tfrac{1}{2}\rho_f (V_0 - \dot{u}_{z0})|V_0 - \dot{u}_{z0}|, \tag{31}$$

where ξ_0 is an empirical loss coefficient (Wylie and Streeter, 1993, pp. 44–45). The same relation is assumed to hold for a closing valve,

$$\Delta P = \xi \tfrac{1}{2}\rho_f (V - \dot{u}_z)|V - \dot{u}_z|, \tag{32}$$

where ξ depends on valve position and hence of time. Division of Eq. (32) by Eq. (31) gives the dimensionless valve closure coefficient $\tau = \sqrt{\xi_0/\xi}$ and the nonlinear boundary condition

$$P_0(V - \dot{u}_z)|V - \dot{u}_z| = \tau^2(t)(V_0 - \dot{u}_{z0})|V_0 - \dot{u}_{z0}|P, \tag{33}$$

in which the pressure downstream of the valve has been taken zero.

The specific function $\tau(t)$ used herein is

$$\tau(t) = \begin{cases} (1 - t/T_c)^{3.53} & \text{for} \quad 0 \leqslant t \leqslant 0.4T_c \\ 0.394(1 - t/T_c)^{1.70} & \text{for} \quad 0.4T_c \leqslant t \leqslant T_c \\ 0 & \text{for} \quad T_c \leqslant t \end{cases} \tag{34}$$

in which T_c is the valve closure time and $\xi_0 = 0.2$ (see Fig. 4). This function, which is based on empirically obtained ball-valve discharge coefficients, see (Lavooij and Tijsseling, 1988, Vol. 1, Appendix A), was provided by Dr. David Wiggert to Delft Hydraulics in 1987. More information on ball-valve discharge characteristics can be found in (Van Rij, 1970; Schedelberger, 1975).

The quadratic Eq. (33) is solved simultaneously with three linear equations (two Riemann invariants and one boundary condition). This is done exactly in Appendix A, which is an update of (Lavooij and Tijsseling, 1988, Vol. 2, Appendix E).

The resistance of the valve in steady state gives a small initial pressure, so that

$$\boldsymbol{\phi}_0 = \begin{pmatrix} V_0 \\ P_0 \\ 0 \\ A_f P_0 / A_s \end{pmatrix}. \tag{35}$$

3. Algorithm

This section with its appendix is the heart of the paper. It describes an algorithm for finding the exact value of the state vector $\boldsymbol{\phi}$ in any point (z, t) in the distance–time plane. The algorithm is formulated in terms of the Riemann

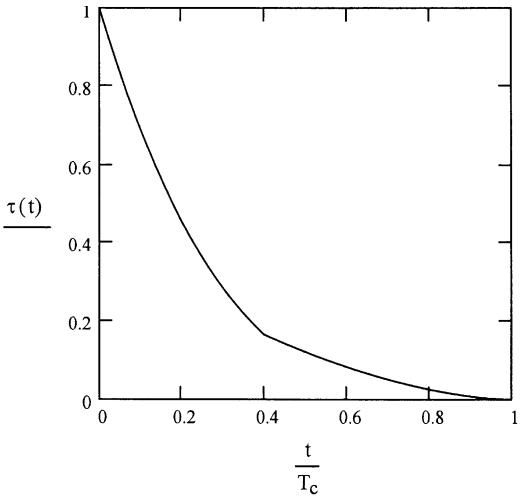

Fig. 4. Valve-closure function $\tau(t)$.

invariants η_i and it is based on a "coast-to-coast" approach, which is explained in words now. Fig. 3 is essential. The vector $\boldsymbol{\eta}$ in point P on the left boundary at $z = 0$ at time t consists of the four components η_1, η_2, η_3 and η_4. The components η_2 and η_4 are assumed to be known because, according to Eq. (17), these are equal to η_2 and η_4 in the points A_2 and A_4, respectively, on the right boundary at $z = L$. The components η_1 and η_3 follow from the boundary conditions (19); they depend on $\mathbf{D}_0$, $\mathbf{S}$, $\mathbf{q}_0$, η_2 and η_4. Naturally, the same story holds for any point P on the right boundary. For the calculation of $\boldsymbol{\eta}$ in point P on the *left* boundary, one needs information from the "earlier" points A_2 and A_4 on the *right* boundary; and for the calculation of $\boldsymbol{\eta}$ in the points A_2 and A_4 on the *right* boundary, one needs information from "earlier" points (e.g., A_1 and A_3) on the *left* boundary. This whole process can nicely be captured in a simple recursion that stops when characteristic lines intersect the $t = 0$ line, at which $\boldsymbol{\eta}$ has a given initial value. The recursion and the treatment of internal points are presented in Appendix B.

4. Results

Some important previous results are recalculated, but now exactly. The exact results give details as fine as the chosen resolution in time and/or distance.

4.1. Wilkinson and Curtis

Wilkinson and Curtis (1980) performed laboratory experiments in a very thin-walled, vertical, steel pipe in which an upward moving water column collided with an unrestrained closed end (Fig. 1). The recorded transient pressure clearly exhibited the occurrence of a precursor wave. Wilkinson and Curtis showed that simplified theory without Poisson coupling was not able to satisfactorily describe the experiment. The more exact FSI four-equation model gave good agreement with the measurement, except for dispersion effects. Unfortunately, the exact solutions given by Wilkinson and Curtis contain errors. For example, and with reference to their Table 2 and their Figs. 8 and 9, the pressure rise caused by the arrival of the precursor wave at the lower transducer is predicted in their table of wave strengths, but not included in the corresponding figure. On the other hand, the doubling of the pressure caused by the reflected precursor wave was predicted well, so that the error is most likely due to the fact that the calculation and the drawing were done by hand. Also, the calculated pressure at the lower transducer is wrong 12 ms after impact. The automated calculation introduced herein gives the results displayed in Fig. 5. The shown pressures at the two transducer positions reveal the small mistakes by Wilkinson and Curtis and they confirm the later simulation by Tijsseling and Lavooij (1989). The data used in the present simulation were: pipe length $L = 6.10$ m, $R = 12.486$ mm, $e = 0.276$ mm, $E = 175.4$ GPa, $\rho_s = 7900\,\mathrm{kg/m^3}$, $\nu = 0.28$, $K = 2.141$ GPa, $\rho_f = 997.5\,\mathrm{kg/m^3}$; the corresponding wave speeds (Eqs. (26)) and their ratio are $\lambda_1 = 1008.9$ m/s, $\lambda_3 = 4816.7$ m/s and $\lambda_3/\lambda_1 = 4.774$. The upper transducer was at $z = 0$ herein, and the lower at $z = 1.2$ m. The initial conditions were zero, except for $V_0 = 5$ m/s.

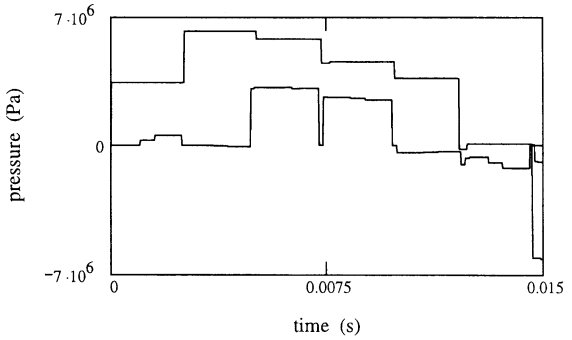

Fig. 5. Exact solutions for the impact test of Wilkinson and Curtis (1980). See Fig. 1. Pressure at impact end (upper transducer, upper line) and pressure 4.90 m away from impact end (lower transducer, lower line).

4.2. Delft Hydraulics Benchmark Problem A

The Delft Hydraulics Benchmark Problems A to F have been defined and used to test numerical methods and FSI software (Tijsseling and Lavooij, 1990; Lavooij and Tijsseling, 1991). Problem A (Fig. 6) concerns a reservoir-pipe-valve system defined by: $L = 20\,\text{m}$, $R = 398.5\,\text{mm}$, $e = 8\,\text{mm}$, $E = 210\,\text{GPa}$, $\rho_s = 7900\,\text{kg/m}^3$, $\nu = 0.30$, $K = 2.1\,\text{GPa}$, $\rho_f = 1000\,\text{kg/m}^3$, $V_0 = 1\,\text{m/s}$, so that the wave speeds (Eqs. (26)) and their ratio are $\lambda_1 = 1024.7\,\text{m/s}$, $\lambda_3 = 5280.5\,\text{m/s}$ and $\lambda_3/\lambda_1 = 5.153$. The instantaneously closing valve may be structurally fixed, implying zero displacement (and velocity), or free and closed, in which case $V = \dot{u}_z$ and $A_f P = A_s \sigma_z$ at the valve. It is noted that the benchmark problems are numerical test cases only; experimental data does not exist.

Fig. 7 shows the dissipative effect of interpolations. The wave speed ratio λ_3/λ_1 (5.153) is close to 5 in this case, so that the interpolation error is relatively small: a ratio of 5.5 will give a stronger smearing of wave fronts. Dr. David Fan (1989) provided the result obtained with (time–line) interpolations.

To avoid interpolations, the author has applied wave speed adjustment in all of his previous work through modified mass densities ρ_f and ρ_s. Fig. 8 shows typical results. If the wave speed ratio is 5/1, 5 structural waves fit in 1 fluid wave. This is nicely exhibited by the broken line, which depicts the pressure at the valve. If the wave speed ratio is 67/13, 67 structural waves fit in 13 fluid waves. This is the more exact solid line. If integer wave speed ratios are employed, the solution cannot converge to the exact solution. If rational wave speed ratios are used, the solution converges when the rational numbers are taken closer to the real number representing the exact wave speed ratio. It is noted that Liou (1983) presented an original method to correct for the adjusted wave speeds. Unfortunately his method introduces some numerical damping.

The algorithm (Mathcad, 2001, worksheet) producing the exact solutions has been verified against existing Fortran code. For rational wave speed ratios λ_3/λ_1, the new algorithm and the old code give practically the same results: the small relative differences of the order of 10^{-7} correspond to the stored precision (7 digits) of the Fortran results. The time used by Mathcad to produce the results in Section 4.1 on a 2 GHz PC was in the order of seconds, but for the results in this Section 4.2 it was in the order of days. The computation time grows exponentially with time t. For example, for $2 < \lambda_3/\lambda_1 < 3$, the number of BOUNDARY calls (see Appendix B) needed to calculate $\boldsymbol{\eta}(P) = \boldsymbol{\eta}(z_b, t)$ is found from a classical Fibonacci sequence.

The new algorithm gives exact waterhammer (without FSI, $\nu = 0$) solutions for the Eqs. (1) and (2)—with σ_z either constant or proportional to P—which is nothing special, except that the exact solutions are not necessarily in equidistantly spaced grid points. The classical waterhammer solutions are used as a reference for the FSI solutions.

If the valve is structurally fixed, the only FSI mechanism is Poisson coupling. The exact pressure at the valve (solid line) in Fig. 9 and the result obtained with a wave speed ratio adjusted to 67/13 are—on this plotting scale—visibly identical, thus confirming the 67/13 result of Tijsseling (1997). The growing pressure amplitude is the result of a beat phenomenon, which also appears in FSI computations of systems with fixed junctions (elbows, branches), see Tijsseling and Heinsbroek (1999), and sometimes in waterhammer measurements (see Budny et al., 1991, Fig. 4a) and Vennatrø (1999, Fig. 16). Fig. 10 displays the pressure at the midpoint ($z = L/2$) obtained with subroutine INTERIOR (see Appendix B).

If the valve is unrestrained, its axial vibration provides a strong mechanism for FSI (junction coupling). The exact pressure at the valve (solid line) in Fig. 11 again confirms the result obtained with a rational wave speed ratio 67/13: one needs to zoom in, as in Fig. 11(top), to see that the differences are small in timing and negligible in magnitude.

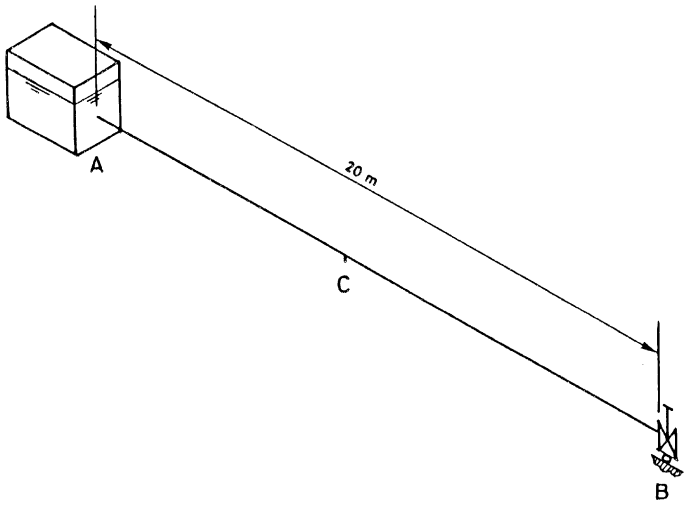

Fig. 6. Reservoir–pipe–valve system in Delft Hydraulics Benchmark Problem A.

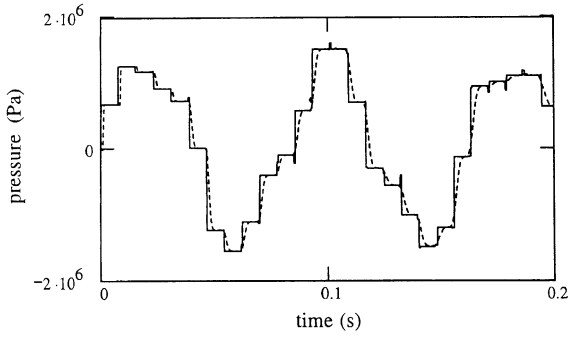

Fig. 7. Effect of interpolations. Pressure at valve for Delft Hydraulics Benchmark Problem A. Solid line: without interpolations, $\Delta z = L$, $\Delta t = 0.29$ ms. Broken line: with interpolations, $\Delta z = L/8$, $\Delta t = 0.47$ ms.

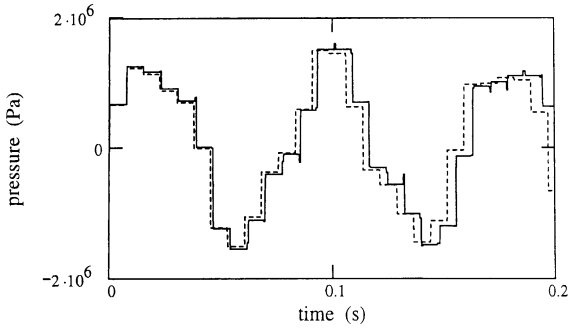

Fig. 8. Effect of wave speed adjustments. Pressure at valve for Delft Hydraulics Benchmark Problem A with *free* valve. Solid line: $\lambda_3/\lambda_1 = 67/13$. Broken line: $\lambda_3/\lambda_1 = 5$.

Fig. 12(lower and top) display the corresponding pressures at the midpoint obtained with subroutine INTERIOR. Each of the FSI graphs in Figs. 8–12 consists of 1374 points.

The results shown so far concern instantaneous valve closure, which is a worst case scenario for industrial systems. The boundary conditions for the valve (Eqs. (29)) were constant, but in conflict with the initial conditions and thus

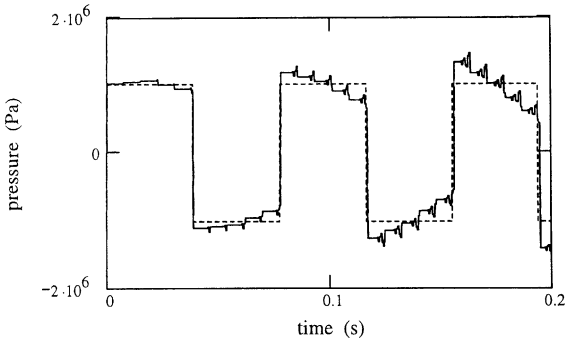

Fig. 9. Poisson coupling. Pressure at valve for Delft Hydraulics Benchmark Problem A with *fixed* valve. Solid line: $\lambda_3/\lambda_1 =$ exact and $\lambda_3/\lambda_1 = 67/13$. Broken line: no FSI.

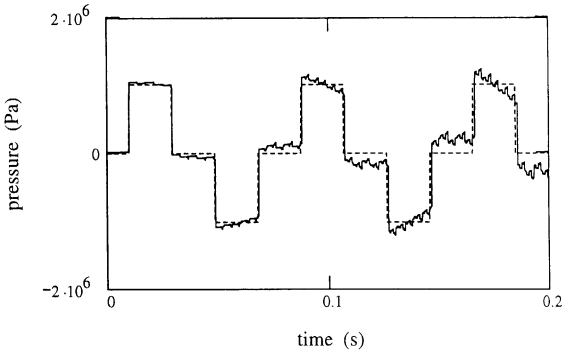

Fig. 10. Poisson coupling. Pressure at midpoint for Delft Hydraulics Benchmark Problem A with *fixed* valve. Solid line: $\lambda_3/\lambda_1 =$ exact and $\lambda_3/\lambda_1 = 67/13$. Broken line: no FSI.

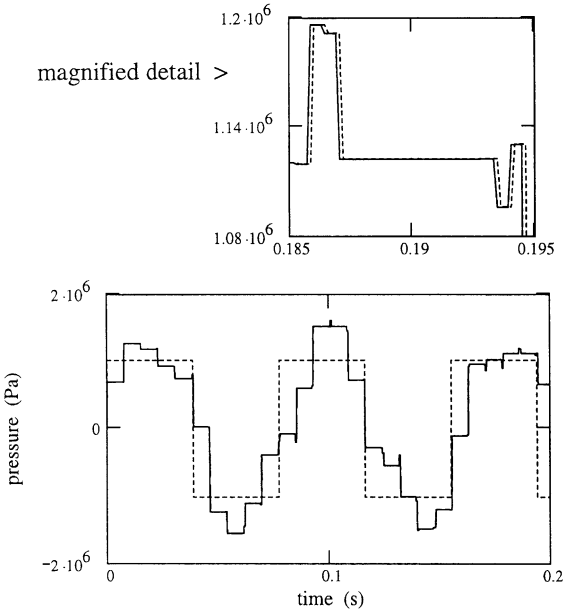

Fig. 11. Poisson and junction coupling. Pressure at valve for Delft Hydraulics Benchmark Problem A with *free* valve. Lower figure: solid line: $\lambda_3/\lambda_1 =$ exact and $\lambda_3/\lambda_1 = 67/13$; broken line: no FSI. The top figure shows a magnified detail not visible in the lower figure: solid line: $\lambda_3/\lambda_1 =$ exact; broken line: $\lambda_3/\lambda_1 = 67/13$.

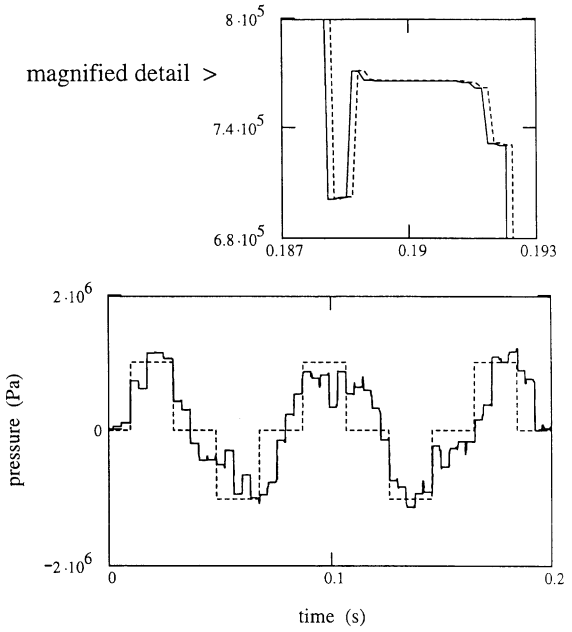

Fig. 12. Poisson and junction coupling. Pressure at midpoint for Delft Hydraulics Benchmark Problem A with *free* valve. Lower figure: solid line: λ_3/λ_1 = exact and $\lambda_3/\lambda_1 = 67/13$; broken line: no FSI. The top figure shows a magnified detail not visible in the lower figure: solid line: λ_3/λ_1 = exact; broken line: $\lambda_3/\lambda_1 = 67/13$.

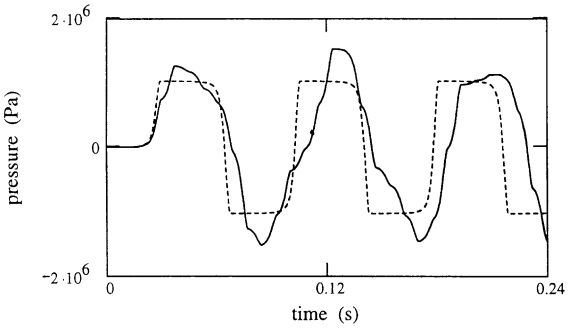

Fig. 13. Non-instantaneous valve closure. Poisson and junction coupling. Pressure at valve for Delft Hydraulics Benchmark Problem A with *free* valve. Solid line: λ_3/λ_1 = exact and $\lambda_3/\lambda_1 = 67/13$. Broken line: no FSI.

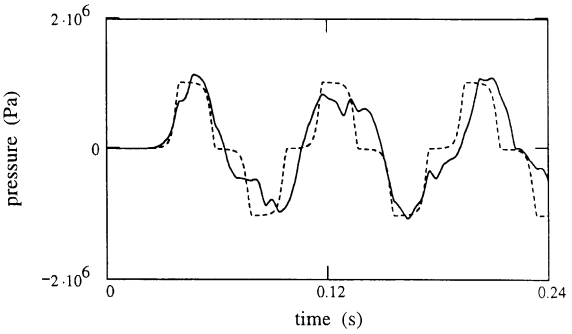

Fig. 14. Non-instantaneous valve closure. Poisson and junction coupling. Pressure at midpoint for Delft Hydraulics Benchmark Problem A with *free* valve. Solid line: λ_3/λ_1 = exact and $\lambda_3/\lambda_1 = 67/13$. Broken line: no FSI.

causing a transient. To show that the new method works for time-dependent boundary conditions, the more realistic case of non-instantaneous valve closure has been calculated. The nonlinear model of Section 2.6 takes $\mathbf{q}_2 = V_r$ in Eq. (30), where V_r is time-dependent and defined by Eq. (A.4). The valve closure time $T_c = 0.03\,\mathrm{s}$ in Figs. 13 and 14. Fig. 13 shows that the pressure effectively starts to rise after time $0.7T_c$. Comparing the FSI results (solid lines) in Figs. 13 and 14 with those in Figs. 11 and 12, one sees that all short-duration pressure spikes have disappeared. Compared with the classical waterhammer (no FSI) solution (broken lines), the extreme pressures are larger and the fundamental frequency is lower. The FSI graphs in Figs. 13 and 14 consist of 825 points.

5. Conclusion

The FSI four-equation model, Eqs. (1)–(4), has been solved exactly for time-dependent boundary and constant (steady state) initial conditions. The strength of the method is the simplicity of the algorithm (recursion) and the fast and accurate (exact) calculation of transient events ($t < 8L/c_f$). Its weakness is the exponential calculation time needed for longer events.

The solutions are exact for the selected points of calculation in the distance–time plane, but they do not give information on what exists in between these points (no guaranteed constant values as in the wave tracking method of Wilkinson and Curtis (1980)). The efficiency of the algorithm can be much improved because many repeat calculations occur, but this will be at the expense of simplicity and clarity. The method is ideal for parallelization and adaptivity.

Appendix A. Solution of nonlinear Eq. (33)

The nonlinear boundary condition (33) is solved simultaneously with three linear equations for the four variables $V_r = V - \dot{u}_z$, P, $\dot{u}_z$ and σ_z. The system of equations can be written as

$$a_1 V_r + a_2 P + a_3 \dot{u}_z + a_4 \sigma_z = a_5, \tag{A.1a}$$

$$b_1 V_r + b_2 P + b_3 \dot{u}_z + b_4 \sigma_z = b_5, \tag{A.1b}$$

$$c_1 V_r + c_2 P + c_3 \dot{u}_z + c_4 \sigma_z = c_5, \tag{A.1c}$$

$$d_1 V_r^2 + d_2 P = d_5, \tag{A.1d}$$

where the coefficients a_i, b_i, c_i and d_i ($i = 1, 2, 3, 4, 5$) can be time dependent and $d_1 \neq 0$.

Elimination of $\dot{u}_z$ and σ_z from the three linear Eqs. (A.1a-c) gives

$$e_1 V_r + e_2 P = e_5. \tag{A.2}$$

For $c_4 \neq 0$ the coefficients e_1, e_2 and e_5 are given below, for $c_4 = 0$ a cyclic interchange ($c_i \to b_i \to a_i \to c_i$) has to be carried out.

$$e_1 = \begin{cases} \textit{singular matrix if } (a_3c_4 - a_4c_3) = 0 \textit{ and } (b_3c_4 - b_4c_3) = 0 \\ (a_1c_4 - a_4c_1) \textit{ if } (a_3c_4 - a_4c_3) = 0 \\ (b_1c_4 - b_4c_1) \textit{ if } (b_3c_4 - b_4c_3) = 0 \\ \dfrac{(a_1c_4 - a_4c_1)}{(a_3c_4 - a_4c_3)} - \dfrac{(b_1c_4 - b_4c_1)}{(b_3c_4 - b_4c_3)} \textit{ otherwise,} \end{cases} \tag{A.3a}$$

$$e_2 = \begin{cases} \textit{singular matrix if } (a_3c_4 - a_4c_3) = 0 \textit{ and } (b_3c_4 - b_4c_3) = 0 \\ (a_2c_4 - a_4c_2) \textit{ if } (a_3c_4 - a_4c_3) = 0 \\ (b_2c_4 - b_4c_2) \textit{ if } (b_3c_4 - b_4c_3) = 0 \\ \dfrac{(a_2c_4 - a_4c_2)}{(a_3c_4 - a_4c_3)} - \dfrac{(b_2c_4 - b_4c_2)}{(b_3c_4 - b_4c_3)} \textit{ otherwise,} \end{cases} \tag{A.3b}$$

$$e_5 = \begin{cases} \text{singular matrix if } (a_3c_4 - a_4c_3) = 0 \text{ and } (b_3c_4 - b_4c_3) = 0 \\ (a_5c_4 - a_4c_5) \text{ if } (a_3c_4 - a_4c_3) = 0 \\ (b_5c_4 - b_4c_5) \text{ if } (b_3c_4 - b_4c_3) = 0 \\ \dfrac{(a_5c_4 - a_4c_5)}{(a_3c_4 - a_4c_3)} - \dfrac{(b_5c_4 - b_4c_5)}{(b_3c_4 - b_4c_3)} \text{ otherwise.} \end{cases} \tag{A.3c}$$

Elimination of P from the two Eqs. (A.1d) and (A.2) gives ($e_2 \neq 0$)

$$V_r = \frac{d_2e_1 \pm [(d_2e_1)^2 - 4d_1e_2(d_2e_5 - d_5e_2)]^{1/2}}{2d_1e_2}. \tag{A.4}$$

Substitution of V_r in Eqs. (A.1a–c) gives three linear equations for P, $\dot{u}_z$ and σ_z, which can easily be solved.

In the present paper the coefficients in Eq. (A.1) are:

$$a_1 = \mathbf{S}_{11}^{-1}, \quad a_2 = \mathbf{S}_{12}^{-1}, \quad a_3 = \mathbf{S}_{13}^{-1} + a_1, \quad a_4 = \mathbf{S}_{14}^{-1}, \quad a_5 = \eta_1(A_1),$$
$$b_1 = \mathbf{S}_{31}^{-1}, \quad b_2 = \mathbf{S}_{32}^{-1}, \quad b_3 = \mathbf{S}_{33}^{-1} + b_1, \quad b_4 = \mathbf{S}_{34}^{-1}, \quad b_5 = \eta_3(A_3),$$
$$c_1 = \mathbf{D}_{41}, \quad c_2 = \mathbf{D}_{42}, \quad c_3 = \mathbf{D}_{43} + c_1, \quad c_4 = \mathbf{D}_{44}, \quad c_5 = \mathbf{q}_4,$$
$$d_1 = \pm 1, \quad d_2 = -\tau^2(t)(V_0 - \dot{u}_{z0})|V_0 - \dot{u}_{z0}|/P_0, \quad d_5 = 0.$$

The definition of a_3, b_3 and c_3 is such that V_r instead of V is the first independent variable in Eq. (20). The matrices $\mathbf{S}$ and $\mathbf{D}$ and vector $\mathbf{q}$ are given in Eqs. (27) and (30).

According to relation (33), which describes positive flow (in z-direction) for positive pressure P, the following condition must hold

$$d_1 V_r \geqslant 0. \tag{A.5}$$

In the example presented in the last paragraph of Section 4.2, $d_1 = +1$ and the + sign (+ root) in Eq. (A.4) gave valid solutions satisfying condition (A.5).

Appendix B. Recursion

B.1. Input

The coefficient matrices $\mathbf{A}$, $\mathbf{B}$, $\mathbf{C}$, $\mathbf{D}(t)$, the excitation vector $\mathbf{q}(t)$, and the initial condition $\boldsymbol{\phi}_0(z)$ describe the complete system in general terms. It is stressed once again that $\mathbf{C} = \mathbf{O}$, so that the algorithm does not apply to Timoshenko beams and systems with distributed friction, viscous damping, etc.

B.2. Output

The output is the state vector $\boldsymbol{\phi} = \mathbf{S}\boldsymbol{\eta}$ as a function of distance and time.

B.3. Boundary points

The subroutine BOUNDARY calculates $\boldsymbol{\eta}$ in the boundary points (see Fig. 3) (finally) from constant initial values. In pseudo-code it reads:

```
BOUNDARY (input: z, t; output: η)
if (t⩽0) then
  η:=η0;
else
  if (z = 0) then
    CALL BOUNDARY (L, t + L / λ4 ; η)
    η4 := η4
    CALL BOUNDARY (L, t + L / λ2 ; η)
    η2 := η2
    η1 := α12(t)η2 + α14(t)η4 + β11(t)q1(t) + β13(t)q3(t)
    η2 := η2
    η3 := α32(t)η2 + α34(t)η4 + β31(t)q1(t) + β33(t)q3(t)
```

Table 1
Definition of the coefficients α and β in subroutine BOUNDARY. $\mathbf{DS}(t)$ is the matrix product of $\mathbf{D}(t)$ and $\mathbf{S}$

$\mathbf{z = 0}$	$\mathbf{z = L}$
$det13(t) : \mathbf{DS}(t)_{1,1} \cdot \mathbf{DS}(t)_{3,3} - \mathbf{DS}(t)_{3,1} \cdot \mathbf{DS}(t)_{1,3}$	$det24(t) : \mathbf{DS}(t)_{2,2} \cdot \mathbf{DS}(t)_{4,4} - \mathbf{DS}(t)_{4,2} \cdot \mathbf{DS}(t)_{2,4}$
$\alpha 12(t) := \dfrac{-(\mathbf{DS}(t)_{1,2} \cdot \mathbf{DS}(t)_{3,3} - \mathbf{DS}(t)_{1,3} \cdot \mathbf{DS}(t)_{3,2})}{det13(t)}$	$\alpha 21(t) := \dfrac{-(\mathbf{DS}(t)_{2,1} \cdot \mathbf{DS}(t)_{4,4} - \mathbf{DS}(t)_{2,4} \cdot \mathbf{DS}(t)_{4,1})}{det24(t)}$
$\alpha 14(t) := \dfrac{-(\mathbf{DS}(t)_{1,4} \cdot \mathbf{DS}(t)_{3,3} - \mathbf{DS}(t)_{1,3} \cdot \mathbf{DS}(t)_{3,4})}{det13(t)}$	$\alpha 23(t) := \dfrac{-(\mathbf{DS}(t)_{2,3} \cdot \mathbf{DS}(t)_{4,4} - \mathbf{DS}(t)_{2,4} \cdot \mathbf{DS}(t)_{4,3})}{det24(t)}$
$\alpha 32(t) := \dfrac{-(\mathbf{DS}(t)_{3,2} \cdot \mathbf{DS}(t)_{1,1} - \mathbf{DS}(t)_{3,1} \cdot \mathbf{DS}(t)_{1,2})}{det13(t)}$	$\alpha 41(t) := \dfrac{-(\mathbf{DS}(t)_{4,1} \cdot \mathbf{DS}(t)_{2,2} - \mathbf{DS}(t)_{4,2} \cdot \mathbf{DS}(t)_{2,1})}{det24(t)}$
$\alpha 34(t) := \dfrac{-(\mathbf{DS}(t)_{3,4} \cdot \mathbf{DS}(t)_{1,1} - \mathbf{DS}(t)_{3,1} \cdot \mathbf{DS}(t)_{1,4})}{det13(t)}$	$\alpha 43(t) := \dfrac{-(\mathbf{DS}(t)_{4,3} \cdot \mathbf{DS}(t)_{2,2} - \mathbf{DS}(t)_{4,2} \cdot \mathbf{DS}(t)_{2,3})}{det24(t)}$
$\beta 11(t) := \dfrac{\mathbf{DS}(t)_{3,3}}{det13(t)} \quad \beta 13(t) := \dfrac{-\mathbf{DS}(t)_{1,3}}{det13(t)}$	$\beta 22(t) := \dfrac{\mathbf{DS}(t)_{4,4}}{det24(t)} \quad \beta 24(t) := \dfrac{-\mathbf{DS}(t)_{1,3}}{det24(t)}$
$\beta 31(t) := \dfrac{-\mathbf{DS}(t)_{3,1}}{det13(t)} \quad \beta 33(t) := \dfrac{\mathbf{DS}(t)_{1,1}}{det13(t)}$	$\beta 42(t) := \dfrac{-\mathbf{DS}(t)_{4,2}}{det24(t)} \quad \beta 44(t) := \dfrac{\mathbf{DS}(t)_{2,2}}{det24(t)}$

```
    η4 := η4
  if (z = L) then
    CALL BOUNDARY (0, t − L/λ3; η)
    η3 := η3
    CALL BOUNDARY (0, t − L/λ1; η)
    η1 := η1
    η1 := η1
    η2 := α21(t)η1 + α23(t)η3 + β22(t)q2(t) + β24(t)q4(t)
    η3 := η3
    η4 := α41(t)η1 + α43(t)η3 + β42(t)q2(t) + β44(t)q4(t)
  if (z≠0 AND z≠L) then
    "z is not at a boundary"
end.
```

Note that λ_2 and λ_4 are negative numbers. The coefficients α and β are given in Table 1. They define the unknowns η_1, η_3 and η_2, η_4 at the left and right boundaries, respectively, as the exact solution of the 2 by 2 linear system of Eqs. (19).

B.4. Interior points

The subroutine INTERIOR calculates $\boldsymbol{\eta}$ in the interior points (see Fig. 2) from the boundary values. In pseudo-code it reads:

```
INTERIOR (input: z, t; output: η)
if (t⩽0) then
  η := η0;
else
  if (0<z<L) then
```

```
    CALL BOUNDARY (0, t − z/λ1; η)
    η1 := η1
    CALL BOUNDARY (L, t − (z − L)/λ2; η)
    η2 := η2
    CALL BOUNDARY (0, t − z/λ3; η)
    η3 := η3
    CALL BOUNDARY (L, t − (z − L)/λ4; η)
    η4 := η4
    η1 := η1
    η2 := η2
    η3 := η3
    η4 := η4
  else
    "z is not an interior point"
end.
```

B.5. Implementation

The algorithm described above has been implemented in Mathcad (2001); the interested reader may find the Mathcad worksheets in (Tijsseling, 2002). For the case of nonlinear non-instantaneous valve closure, as described in Section 2.6, in subroutine BOUNDARY: $q_2(t) = V_r$, Eq. (A.4), for $z = L$.

References

Bergant, A., Tijsseling, A.S., 2001. Parameters affecting water hammer wave attenuation, shape and timing. In: Brekke, H., Kjeldsen, M. (Eds.), Proceedings of the 10th International Meeting of the IAHR Work Group on the Behaviour of Hydraulic Machinery under Steady Oscillatory Conditions. Trondheim, Norway, Paper C2, pp. 1–12.

Bouabdallah, S., Massouh, F., 1997. Fluid–structure interaction in hydraulic networks. In: Païdoussis, M.P. (Ed.), Proceedings of the 4th International Symposium on Fluid–Structure Interactions, Aeroelasticity, Flow-Induced Vibration and Noise. Dallas, USA, ASME-AD 53-2, pp. 543–548.

Budny, D.D., Wiggert, D.C., Hatfield, F.J.B., 1991. The influence of structural damping on internal pressure during a transient flow. ASME Journal of Fluids Engineering 113, 424–429.

Bürmann, W., 1975. Water hammer in coaxial pipe systems. ASCE Journal of the Hydraulics Division 101, 699–715 (Errata in 101, 1554.).

Bürmann, W., Thielen, H., 1988a. Study on the motion of the filling string of a saline cavern. 3R International 27, 275–281 (in German).

Bürmann, W., Thielen, H., 1988b. Measurement and computation of dynamic reactive forces on pipes containing flow. 3R International 27, 434–440 (in German).

Bürmann, W., Feser, G., Janson, H., Thielen, H., 1987. Pressure and acceleration measurements on the pipe bridge of a long-distance water main to study the piping dynamics in case of unsteady flow. 3R International 26, 638–646 (in German).

Edwards, N.A., Please, C.P., 1988. An assessment of the moving point method for numerical calculation of fluid–structure interaction in water hammer. Central Electricity Generating Board (CEGB) Research Report TPRD/L/3258/R88 (Obtainable from National Power PLC, Whitehill Way Swindon, Wiltshire SN5 9NX, UK).

Elansary, A.S., Contractor, D.N., 1990. Minimization of stresses and pressure surges. ASME Journal of Pressure Vessel Technology 112, 311–316.

Fan, D., 1989. Fluid–structure interactions in internal flows. PhD Thesis, The University of Dundee, Department of Civil Engineering, Dundee, UK.

Lavooij, C.S.W., Tijsseling, A.S., 1988. FLUSTRIN Phase 1—Fluid–structure interaction in MDOF pipe systems. Report J0252/J0284, Vol. 1: Results, May 1988, Vol. 2: Theory, June 1988, Delft Hydraulics, Delft, The Netherlands.

Lavooij, C.S.W., Tijsseling, A.S., 1991. Fluid–structure interaction in liquid-filled piping systems. Journal of Fluids and Structures 5, 573–595.

Liou, C.P., 1983. Calculations of transients in batched pipelines. In: Stephens, H.S., Jarvis, B., Goodes, D. (Eds.), Proceedings of the 4th International Conference on Pressure Surges, BHRA, Bath, UK, pp. 13–25.

Mathcad, 2001. Mathcad, 2001*i*, User's Guide. MathSoft Engineering & Education, Inc., Cambridge, USA.

Rij, A.A.van, 1970. Standaard afsluiterkarakteristieken (Standard valve characteristics). Delft Hydraulics Laboratory, Report V 195, October 1970, Delft, The Netherlands (in Dutch).

Schedelberger, J., 1975. Closing characteristics of spherical valves. 3R International 14, 333–339 (in German).

Schwarz, W., 1978. Druckstoßberechnung unter Berücksichtigung der Radial- und Längsverschiebungen der Rohrwandung (Waterhammer calculations taking into account the radial and longitudinal displacements of the pipe wall). PhD Thesis, Universität Stuttgart, Institut für Wasserbau, Mitteilungen, Heft 43, Stuttgart, Germany, ISSN 0343-1150 (in German).

Skalak, R., 1955/1956a. An extension of the theory of waterhammer. Water Power, 7(458–462)/8(17–22).

Skalak, R., 1956b. An extension of the theory of waterhammer. Transactions of the ASME 78, 105–116.

Tijsseling, A.S., 1993. Fluid–structure interaction in case of waterhammer with cavitation. PhD Thesis, Delft University of Technology, Faculty of Civil Engineering, Communications on Hydraulic and Geotechnical Engineering, Report No 93-6, ISSN 0169-6548, Delft, The Netherlands.

Tijsseling, A.S., 1996. Fluid–structure interaction in liquid-filled pipe systems: a review. Journal of Fluids and Structures 10, 109–146.

Tijsseling, A.S., 1997. Poisson-coupling beat in extended waterhammer theory. In: Païdoussis, M.P. (Ed.), Proceedings of the 4th International Symposium on Fluid–Structure Interactions, Aeroelasticity, Flow-Induced Vibration and Noise. Dallas, USA, ASME-AD 53–2, pp. 529–532.

Tijsseling, A.S., 2002. Exact solution of the FSI four-equation model. Research Report RANA 02–16, Department of Mathematics and Computer Science, Eindhoven University of Technology, Eindhoven, The Netherlands, ISSN 0926-4507.

Tijsseling, A.S., Heinsbroek, A.G.T.J., 1999. The influence of bend motion on waterhammer pressures and pipe stresses. In: Liou, J.C.P. (Ed.), Proceedings of the 3rd ASME & JSME Joint Fluids Engineering Conference, Symposium S-290 Water Hammer, San Francisco, USA, ASME–FED 248, Paper FEDSM99-6907, ISBN 0-7918-1961-2 (CD-ROM) or ISBN 0-7918-1978-7.

Tijsseling, A.S., Lavooij, C.S.W., 1989. Fluid–structure interaction and column separation in a straight elastic pipe. In: Thorley, A.R.D. (Ed.), Proceedings of the 6th International Conference on Pressure Surges, BHRA. Cambridge, UK, pp. 27–41.

Tijsseling, A.S., Lavooij, C.S.W., 1990. Waterhammer with fluid–structure interaction. Applied Scientific Research 47, 273–285.

Tijsseling, A.S., Vardy, A.E., Fan, D., 1996. Fluid–structure interaction and cavitation in a single-elbow pipe system. Journal of Fluids and Structures 10, 395–420.

Vardy, A.E., Fan, D., 1989. Flexural waves in a closed tube. In: Thorley, A.R.D. (Ed.), Proceedings of the 6th International Conference on Pressure Surges, BHRA. Cambridge, UK, pp. 43–57.

Vennatrø, R., 1999. Measurement of velocity profiles in waterhammer and steady oscillatory flow in a rigid steel pipe. In: Pulpitel, L. (Ed.), Proceedings of the 9th International Meeting of the IAHR Work Group on the Behaviour of Hydraulic Machinery Under Steady Oscillatory Conditions. Brno, Czech Republic, Paper C5, pp. 1–12 + discussion.

Wiggert, D.C., Tijsseling, A.S., 2001. Fluid transients and fluid–structure interaction in flexible liquid-filled piping. ASME Applied Mechanics Reviews 54, 455–481.

Wiggert, D.C., Otwell, R.S., Hatfield, F.J., 1985. The effect of elbow restraint on pressure transients. ASME Journal of Fluids Engineering 107, 402–406.

Wiggert, D.C., Hatfield, F.J., Stuckenbruck, S., 1987. Analysis of liquid and structural transients by the method of characteristics. ASME Journal of Fluids Engineering 109, 161–165.

Wilkinson, D.H., Curtis, E.M., 1980. Water hammer in a thin-walled pipe. In: Stephens, H.S., Hanson, J.A. (Eds.), Proceedings of the 3rd International Conference on Pressure Surges, BHRA. Canterbury, UK, pp. 221–240.

Williams, D.J., 1977. Waterhammer in non-rigid pipes: precursor waves and mechanical damping. IMechE Journal of Mechanical Engineering Science 19, 237–242.

Wylie, E.B., Streeter, V.L., 1993. Fluid Transients in Systems. Prentice Hall, Englewood Cliffs, NJ, USA.

Zhang, X., Huang, S., Wang, Y., 1994. The FEM of fluid structure interaction in piping pressure transients. In: Fiedler, H.E., Lee, B.H.K. (Ed.), Proceedings of the First International Conference on Flow Interaction. Hong Kong, pp. 532–535.

Zhang, L., Tijsseling, A.S., Vardy, A.E., 1999. FSI analysis of liquid-filled pipes. Journal of Sound and Vibration 224 (1), 69–99.